CrystEngComm

Accepted Manuscript

ROYAL SOCIETY OF CHEMISTRY

www.rsc.org/crystengcomm

A crucial process: organic matrix and magnesium ion control amorphous calcium carbonate crystallization on ß-chitin film

Yufei Ma [a, b] and Qingling Feng [* c, d]

Amorphous calcium carbonate (ACC) particles with diameter of about 300 nm were synthesized first. Then the as-prepared products were used to investigate ACC transformation processes occurring on chitin film under the control of water soluble matrix (WSM, extracted from aragonite pearl, China) or magnesium ion in aqueous solution respectively. Raman spectroscopy, transmission electron microscopy (TEM) together with selected area electron diffraction (SAED) and field-emission scanning electron microscopy (FE-SEM) equipped with energy-dispersive X-ray (EDX) were used to characterize the crystallized calcium carbonate from ACC. These results demonstrate that the existence of WSM and chitin film offers the ability to control the pure aragonite phase, leading to the rod-like aragonite crystal aggregates. Comparatively, the collaborative effect of magnesium ion and chitin film not only induces to form the aragonite crystal aggregates, but also inhibits the transformation from ACC to Mg-calcite. Moreover, a possible transformation mechanism has been proposed and discussed.

1. Introduction

Calcium carbonate ($CaCO_3$) is one of the most important industrial and biological materials due to its abundance in nature and its wide applications in industry. In parallel, $CaCO_3$ can be used as a

[a] *MOE Key Laboratory of Biomedical Information Engineering, School of Life Science and Technology, Xi'an Jiaotong University, Xi'an, 710049, PR China*
[b] *Bioinspired Engineering and Biomechanics Center, Xi'an Jiaotong University, Xi'an 710049, PR China*
[c] *State key laboratory of new ceramics and fine processing, Department of Materials Science and Engineering, Tsinghua University, Beijing 100084, China*
[d] *Laboratory of Advanced Materials, Department of Materials Science and Engineering, Tsinghua University, Beijing 100084, China. E-mail: biomater@mail.tsinghua.edu.cn (Qingling Feng);Tel: +86-10-62782770; Fax: +86-10-62771160*

model mineral for biomimetic research, by which biogenic control over mineral orientation, polymorph and morphology has been intensively studied.[1] Additionally, many *in vitro* studies have focused on unraveling biomineralization mechanisms in the hope to mimic the natural materials and to control the material structures and properties. Calcium carbonate in nature has three anhydrous crystalline polymorphs (calcite, aragonite and vaterite), and two well-defined hydrous crystalline polymorphs, calcium carbonate monohydrate ($CaCO_3 \cdot H_2O$) and calcium carbonate hexahydrate ($CaCO_3 \cdot 6H_2O$), as well as one amorphous form.[2]

Amorphous calcium carbonate (ACC) is a hydrated, poorly ordered and metastable precursor to crystalline calcium carbonate. Many research results illustrate that ACC is a useful amorphous phase for many aspects and plays an important role in the biomineralization of $CaCO_3$.[3, 4] ACC is found in various organisms such as mature sea urchin larvae[4, 5] and larvae of molluscan bivalves.[6] On the other hand, ACC is used as temporary storage deposits and structural skeletal elements,[7-9] and acts as transient precursors to the crystalline polymorphs.[8, 10, 11] The rich variety of $CaCO_3$ structures in nature may be due to the character of ACC, which is easily molded into many different shapes. Thus, it is of scientific and industrial interest to study the transformation mechanism from ACC to crystal. Despite its importance, however, there are few reports on ACC due to its unstable nature.

Previously, a simple route containing a low temperature and in the presence of a high amount of magnesium was used to synthesize highly monodispersed spherules of ACC in the lab firstly.[12] Additionally, two solutions, (I) an aqueous solution including Ca^{2+} ions and dimethyl carbonate (DMC) and (II) an aqueous NaOH solution, were required to prepare ACC particles.[13] However, stabilization and crystallization of ACC are controlled by various factors, including temperature,

pH, additive and solvent.[14-17] Sawada has reported that ACC precipitated at lower temperatures is more stable, whereas an increasing precipitation temperature induces crystallization.[14] Koga et al. found that an increasing alkalinity stabilizes the amorphous state and then this observation was quantified by determining enthalpies for the transformation of ACC into calcite in dependence of the pH of the mother liquor.[15] Recently, various additives have been used as stabilizers for ACC, such as magnesium ion,[16, 18, 19] phosphate,[14, 20] polyglutamates and DNA,[21-23] and the transformation of ACC has been investigated. Loste et al. [24] reported that ACC was the first phase formed in aqueous solution containing magnesium ions. The magnesium content of the ACC was determined by the Mg:Ca ratio in the solution, and increased systematically with the increasing Mg:Ca. Then the crystalline phase produced by the transformation of ACC depended on the magnesium content of ACC. Additionally, several research groups have studied the use of mixtures of different solvents to control the transformation of ACC or the crystallization of calcium carbonate.[17, 25-27] Chen et al.[17, 25] reported water-induced phase transformation of poly (4-sodium styrene sulfonate) or poly (acrylic acid) stabilized ACC in water−ethanol solution at room temperature. Liu et al. [28] described that the phase transformation of magnesium amorphous calcium carbonate could be easily realized in an ethanol/water mixed solution free from organic additives under mild conditions. Though each factor mentioned above has been investigated independently on its influence of ACC stabilization and transformation, the combined effect on ACC crystallization is more closed to the complicated biomineralization process in nature, and the real ACC transformation detail is poorly understood until now.

Recently, increasing evidences prove that biomineralization occurs through self-assembly and/or transformation of amorphous precursor, such as in the case of sea urchins spines[29, 30] and

oyster shells.[31-33] Weiss et al. [6] has reported that initially deposited mineral phase of mollusc larval shell is predominantly amorphous calcium carbonate, that subsequently partially transforms into aragonite. Nassif et al. [34] recently demonstrated that the nacreous tablets of adult mollusk shell nacre are coated by a thin surface layer of ACC. These studies suggest that the primary minerals are likely amorphous. The transient formation of ACC seems to be a general principle in biomineralizaiton. In different invertebrates, chitin could be regarded as the substrate that binds other macromolecules, which in turn induce nucleation of mineral phase. This is well described for mollusc shells, specifically for nacre, where chitin has been suggested as an important component of the molluscan organic matrix.[35] Hence, chitin, as a common substrate, plays an important role in $CaCO_3$ crystal growth. However, limited information is available on the effect of chitin on ACC transformation and crystallization.

In biological systems, both Mg and specialized organic macromolecules may be used to stabilize ACC.[36] Previously, we reported that water soluble matrix of aragonite pearl from *hyriopsis cumingii* had ability to induce aragonite crystals.[37] In the present work, ACC particles are synthesized first. Then we perform a systematic study of the transformation process from ACC to crystalline phases on chitin film under the control of WSM or magnesium ion in aqueous solution. The phase transformation of ACC is observed during the formation of the rod-like and the quasi-spherical aragonite aggregates, and a possible growth mechanism of the aragonite crystal aggregates with different morphologies has been proposed. Moreover, this study could also be used in the rational design of new materials with complex shapes assembled from precursor or stable amorphous structures.

2. Experimental

2.1 Materials

All chemicals are analytical grade. Calcium chloride dehydrate, magnesium chloride hexahydrate, sodium hydroxide, dimethyl carbonate, ethanol and acetone were obtained from Sinopharm Chemical Reagent Company and used without further purification. Chitin was purchased from Shanghai Chemical Reagent Company and cut into small pieces (area: ~1 cm^2). Double-distilled water was used throughout the experimental process.

2.2 Synthesis of Amorphous Calcium Carbonate (ACC)

0.147 g $CaCl_2 \cdot 2H_2O$ and 421 μl dimethyl carbonate dissolved in 80 ml water were placed in the beaker at 4 °C. The reaction was started by adding 20 ml 0.5 M sodium hydroxide to the reaction solution under stirring. After 2 min the precipitate was removed from the reaction mixture by centrifugation, then washed with acetone and ethanol and dried at 30 °C.[38, 39]

2.3 Effects of organic matrix and magnesium ion on ACC crystallization on chitin film

WSM of aragonite pearl from *hyriopsis cumingii* was extracted[40] and prepared in the solution with the concentration of 100 ug/ml. Magnesium chloride solutions (10 mM and 40 mM) were prepared and named as low Mg solution and high Mg solution respectively. In the experiment group, 10 mg ACC was immersed in 20 ml WSM and Mg ion solutions respectively. In the control group, 10 mg ACC was immersed in 20 ml water. Silicon slice and the prepared chitin film were used as the substrates for calcium carbonate crystal growth. Mineralization process lasted for 12 h at room temperature. Finally, the substrates with deposited $CaCO_3$ crystals were taken from the

solution carefully, washed with double-distilled water and dried for characterization. For the time-dependent crystallization study, the substrates were removed from the mineralization system at the designed time.

2.4 Characterization

Morphology and elemental composition of calcium carbonate crystals were observed on a field-emission scanning electron microscope (FESEM, JSM-7001F) with energy-dispersive X-ray (EDX, Oxford Instruments). Transmission electron microscope (TEM, JEOL-2011) operated at 200 KV together with selected area electron diffraction (SAED) were used to determine polymorph. Amorphism of calcium carbonate was identified by X-ray powder diffraction (XRD, D8 ADVANCE) with Cu Kα radiation (40 kV, 40 mA) and Fourier transform infrared spectrometer (FT-IR, Nicolet 6700) from 4000 to 400 cm^{-1} at room temperature by the KBr pellets method. Thermogravimetric analysis-mass spectrometry (TGA-MS) curves were measured under argon on a Mettler Todedo ThermoSTAR TGA/SDTA 851. Raman spectroscopy (RM 2000) was used to confirm the polymorph of the deposited $CaCO_3$. Some typical crystals that could represent the overall situation were selected to analyze separately by Raman spectrometer with the Raman shifts ranging from 100 to 1200 cm^{-1}, an argon ion laser at a wavelength of 613 nm was used.

3. Results and discussion

3.1 Characterization of ACC particles

The synthesized calcium carbonate was characterized by SEM, X-ray diffraction, FTIR and TGA-MS. Calcium carbonate synthesized by using $CaCl_2 \cdot 2H_2O$, DMC and NaOH is completely

consisted of spherical particles with diameter of about 300 nm and the surface of particles looks smooth (Fig. 1a). X-ray diffraction pattern reveals some broad bumps located at a 2θ of ~30° and ~45° (Fig. 1b), which reflects the poorly ordered nature of the solid. In addition, there also appears two little peaks at a 2θ of 29.5° and 47.7°. This indicates that small amounts of calcite are present in these poorly ordered solid (ICDD PDF 05-586). Furthermore, there are broad and strong absorption peaks at 866 cm^{-1}, accompanying with a split peak at 1420 and 1475 cm^{-1} in FT-IR spectra (Fig. 1c). ACC has a characteristic broad ν2 absorption band at ~866 cm^{-1}, and a split peak at ~1418 and 1475 cm^{-1}.[8] Hence, it also shows that the overwhelming majority of calcium carbonate particles are amorphous. Actually, Ajikumar et al.[12] first described a simple and efficient strategy for the synthesis of monodispersed microspheres of ACC by using a low-temperature precipitation of calcium carbonate without any organic additives. The endothermic process at 89 °C and 140 °C is proved to be loss of water, identified by thermogravimetric analysis-mass spectrometry (Fig. 1d). Water is lost in two distinct steps. From 65 to 120 °C, a first step is assigned to loosely bound water. In the second step from 120 to 250 °C, structural water is lost with concurrent formation of calcite. Water stabilizes the amorphous phase, and if water is completely removed, crystallization occurs.[8, 41] Finally, at around 500 °C, the sample decomposes to calcium oxide and carbon dioxide.

3.2 Effect of WSM from freshwater pearl on ACC crystallization on chitin film

ACC crystallized by soaking ACC powders into the solution with or without WSM on silicon slice and chitin film, respectively. The precipitated $CaCO_3$ crystals, leading to the formation of calcite and aragonite, were determined by Raman spectroscopy (Fig. 2). Inset in each figure shows the

morphology of the analyzed crystal which represents the overall crystals. The peaks at 283 cm^{-1}, 713 cm^{-1} and 1087 cm^{-1} are characteristic peaks of calcite. While the peaks at 154 cm^{-1} and 206 cm^{-1} are due to the typical Raman spectral lines of aragonite.[42] Furthermore, according to the previous study, a pair of peaks at 700 cm^{-1} and 704 cm^{-1} is characteristic of aragonite,[43, 44] which is also observed in our Raman data (Fig. 2e and f). For aragonite, the site symmetry of the CO_3^{2-} ion causes the two doubly degenerate v_4 in-plane bending modes to split into a pair of non-degenerate modes.[45]

ACC mineralization occurs on the surface of silicon slice and chitin film. In the absence of WSM, only calcite is formed either on silicon slice or on chitin film despite the difference in the crystal morphology. Calcite crystals with the exposed (104) crystalline faces grow on silicon slice (Fig. 3a), and the irregular spherical calcite are observed on the chitin film (Fig. 3b). This is attributed to the different substrates and there exists an interaction between $CaCO_3$ crystals and the chitin film. Some amino groups are existed in chitin macromolecule.[46] Hence, the interaction between $–NH^{3+}$ in chitin macromolecule and CO_3^{2-} could affect calcium carbonate crystallization, which leads to the irregular calcite formation. Liu et al.[47] grafted the different kinds of the functional groups on monocrystalline silicon chips to study their effects on calcium carbonate crystallization and they found that the amount of the typical calcite with (104) crystalline faces was dramatically decreased on $–NH_2$ modified substrates. This could be due to the inhibiting effect of amino groups on (104) crystalline faces. Consequently, only chitin film has an effect on $CaCO_3$ morphology rather than the polymorph. Incorporating WSM into the crystallization procedure leads to a significant change in crystal polymorph. Introducing WSM into the mineralization solution results in the formation of aragonite accompanied by calcite on silicon

slice (Fig. 3c). In contrast, the rod-like aragonite crystals predominantly grow when the template is chitin film (Fig. 3d). The trigger for inducing the formation of aragonite, the polymorph in nacre, is therefore the additive of WSM from the freshwater pearl. WSM possesses rich carboxylic groups.[48] Interfacial interaction between the functional groups of WSM and the ions in the solution can reduce nucleation energy of aragonite, which is responsible for the formation of aragonite crystals.[37] Although WSM additive alone has the capacity to induce aragonite, the combination of chitin film and WSM enhances significantly the amount of aragonite. Hence, the combination of WSM with chitin film can offer the ability to synthetically control the pure aragonite phase.

3.3 Effect of magnesium ion on ACC crystallization on chitin film

To investigate the effect of magnesium ion on ACC mineralization, ACC powder was immersed in low Mg solution (10 mM) and high Mg solution (40 mM) respectively. ACC crystallization took place on silicon slice or chitin film. When ACC crystalized in low Mg solution on silicon slice, a majority of spindle-like aragonite aggregates composed of little needle-like crystals were observed (Fig. 4a), accompanying with some irregular Mg-calcite determined by Raman spectroscopy (Fig. 2b). The spectrum exhibits that the band characteristics [two lattice modes at 158 and 284 cm^{-1}, respectively, ν_1 (CO_3^{2-}) symmetric stretching at 1090 cm^{-1} and ν_4 (CO_3^{2-}) antisymmetric bending at 716 cm^{-1}] are similar to the respective values of Mg-calcite reported in the previous work.[38] The observed shift of positions of carbonate anion fundamentals towards higher wavenumbers results from higher cation (Mg^{2+}) polarizing power in comparison to that of Ca^{2+} in pure calcite.[49] In contrast, ACC crystallization on chitin film leads to the formation of the rod-like aragonite

aggregates only (Fig. 4b). The crystalized calcium carbonate obtained in high Mg solution on silicon slice is shown in Fig. 4c. Some quasi-spherical aragonite aggregates appear, coexisting with a few Mg-calcites (Fig. 4c). Each quasi-spherical aragonite aggregate is also made up of the needle-like crystals. Comparatively, only quasi-spherical aragonite aggregates are obtained on chitin film without other calcium carbonate polymorph (Fig. 4d). Hence, it is concluded that the formation of the spindle-like aragonite aggregates, the rod-like aragonite aggregates, the quasi-spherical aragonite superstructures and the irregular Mg-calcite all come from the transformation of ACC precursor.

It is well known that ACC is easier to be dissolved in the solution and thereby rapidly transforms into calcium carbonate crystals in ambient conditions in the absence of any additives.[4, 50] Magnesium ion, as a cosolute of calcium, has higher hydration energy, and dehydration of the magnesium ions prior to incorporation in the calcite lattice creates a barrier to the growth of calcite nuclei.[24] This is the reason why aragonite crystals can be obtained more easily in the presence of sufficient magnesium. Noteworthily, magnesium ion just induces the formation of aragonite in which magnesium is not incorporated.[51] The previous report also has demonstrated that via control of polymer or biomolecules, a mixture of aragonite with Mg-calcite was obtained by ACC crystallization in aqueous solution.[22]

Mg-ACC nanoparticles serve as the intermediate precursor for the formation of Mg-calcite crystal, which is also a very popular transformation process for the biogenic calcite minerals.[34, 52, 53] For instance, Long et al.[54] synthesized the high-magnesium calcite via polymer-stabilized amorphous calcium magnesium carbonate precursors under mild conditions. This in vitro fabrication of high-magnesium calcite provided some indirect clues to the formation mechanism

of biogenic Mg-calcite. Mg^{2+} ion can incorporate into the structures of calcite. Additionally, Mg^{2+} ion is more strongly hydrated than Ca^{2+} ion and is specifically adsorbed on the crystal faces of calcite, producing crystals elongated along the *c* axis,[55] which results in a pronounced morphology change compared with the typical rhombohedra morphology of calcite. A trend was found that aragonite morphology changed from rod-like aggregate to quasi-spherical aggregate with an increase in mg^{2+} ion concentration, which indicated that magnesium ions acted as a shape modifier in our experiment. The existence of Mg-calcite was determined by the substrate on which ACC crystallization happened. On chitin film, no Mg-calcite crystals grew in low Mg and high Mg solutions either. Therefore, we believe that the combination of magnesium ion and chitin substrate not only induces aragonite crystals growth but also inhibits the transformation from ACC to Mg-calcite.

3.4 Process of ACC crystallization under the control of organic matrix or magnesium ion on chitin film

Time-dependent morphology evolution process was carefully examined to understand the formation process of ACC crystallization under the control of WSM or magnesium ion on chitin film (Fig. 5). Initially, ACC precursor with the diameter of ~300 nm are obtained (Fig. 5a) by separating it from the mother solution and washing with ethanol and acetone, because the amorphous phase is very unstable in aqueous solution. The sample precipitated on chitin film after 6 h under the control of WSM is shown in Fig. 5b. There exist some aragonite crystal aggregates with rod-like shape and some other ACC particles. The existence of ACC indicates that WSM has the capacity to stabilize ACC in aqueous solution. The diameter and length of aragonite crystal

aggregate are about 1 μm and 3 μm, respectively. Each rod-like aragonite crystal aggregate is composed of the needle-like crystals. After 12 h, all ACCs crystalize to form aragonite crystals and the pre-existing aragonite crystal aggregates grow bigger with the length of ~5 μm and the diameter of ~1.8 μm (Fig. 5c). When magnesium ion as a kind of additive was added into the solution, the transformation process from ACC into aragonite crystal aggregate differed from that with the additive of WSM. Magnesium ions diffused and presented within the structure of ACC and thus changed the morphology from the spherical shape into the ellipsoid-like morphology after 2 h (Fig. 5d). It led to the formation of Mg-ACC proved by energy-dispersive X-ray (Fig. 5g) and TEM with selected area electron diffraction (Fig. 5h). SAED pattern shows that the sample is still in the amorphous state and EDX analysis result shows the co-existence of calcium, magnesium, oxygen and carbon (Fig. 5g), which indicates that the ACC contains magnesium. With prolonged time, this ellipsoid-like Mg-ACC disappeared and many needle-like aragonite primary crystals with the length of ~750 nm grew on chitin film after mineralization for 6 h (Fig. 5e). Previous work reported that the growth of aragonite was preferred along the *c* axis.[56] As a result of that, under normal temperature and pressure, aragonite crystal constructs as fine needle. When the mineralization time reached 12 h, the rod-like aragonite crystal aggregates (length: ~5 μm) appeared on chitin film in 10 mM magnesium ion solution (Fig. 5f) while the quasi-spherical aragonite aggregates (diameter: ~6 μm) grew in 40 mM magnesium ion solution (Fig. 5i).

On the basis of the above results and analyses, the possible mechanism of ACC crystallization on chitin film under the control of WSM (Fig. 6a) or magnesium ion (Fig. 6b) are proposed and simply illuminated. When WSM was added in the solution, firstly, WSM adsorbed on the surface of ACC particles to form the WSM stabilized ACC. In this case, some ACC particles with the

original size were still observed after 6 h in the solution (Fig. 5b). Hence, WSM inhibited the dissolution of ACC so that the dissolution-recrystallization process rarely took place. It is concluded that a solid-solid phase transformation is the primary mechanism for ACC crystallization under the control of WSM. Previous literature reported that ACC had a short-range order structure.[8] This short-range order structure might function as the basic unit that reconstructed into the corresponding crystalline form. The local centers of the ordered structure aligned and coalesced cooperatively to form crystalline microdomains. As the mineralization time went on, these crystalline microdomains grew and coalesced continually, leading to the formation of needle-like primary crystal. Subsequently, new ACC particles deposited on the surface of the needle-like primary crystals and then transformed into crystal forms. Tang et al. [57] believed this surface nucleation and subsequent growth, and transformation of ACC happened at the same time. The nucleation and growth of new primary crystals on the surface of the pre-formed crystal resulted in the uniting of adjoining primary crystals and eventually the rod-like crystal aggregate formed.

In contrast, the process of ACC crystallization on chitin film under the control of magnesium ion is quite different (Fig. 6b). When Mg^{2+} ions were introduced in the mineralization system, Mg-ACC with the ellipsoid-like morphology appeared (Fig. 5d). In the previous studies, some Mg-ACC with the imperfect spherical morphologies was reported but the specific reason was still unclear.[20, 54, 58, 59] Hence, we suppose that mg^{2+} ions adsorbed on ACC initially and then entered into the structure of ACC, which led to the ellipsoid-like morphology. The role that magnesium may play in the control of ACC stabilization should be considered. Recently, the high dehydration energy of magnesium ion has been considered to be responsible for the effect of magnesium ion in

stabilizing ACC.[39] Magnesium present within the structure of ACC is likely to prevent its dehydration, hence reducing the rate of dissolution and decreasing its overall solubility.[60] This decrease in solubility reduces the supersaturation in the solution, which is the possible reason for Mg-ACC stabilization. Additionally, another factor also contributes to explain how magnesium ion stabilizes the amorphous state. Bond lengths around Mg are expected to be shorter relative to Ca-O bond lengths.[61] Some literature reported that the Mg-O bond lengths measured in ACC were even shorter compared to the crystalline Mg carbonate minerals.[62] This indicates that magnesium ion in ACC is not influenced by the host ACC phase. Thus, the presence of magnesium ion in ACC causes significant distortion of the local atomic structure, favoring a disordered atomic structure of the bulk and consequently stabilizing the amorphous phase. Therefore, in the present work, Mg-ACC disappeared till 6 h and the needle-like aragonite primary crystals formed (Fig. 5e). With prolonged time, the needle-like primary crystals joined together by aggregation to become larger rod-like crystal aggregates in the solution with low Mg ion concentration (Fig. 5f). Comparatively, in high Mg ion concentration solution, this kind of needle-like primary crystals first integrated into the cross-linked crystal aggregates. Then, the needle-like primary crystals continued to be attracted, joined and attached onto the cross-linked crystal aggregates to produce uniform quasi-spherical crystal aggregates (Fig. 5i). The growth process of $CaCO_3$ crystals along with the morphological change has been observed for other similar structures such as "dumbbell"[63] and "peanut"[57, 64] morphologies. Despite all this, it must be pointed out that the exact mechanism for ACC crystallization with different morphologies is extremely complicated and needed to be further studied.

4. Conclusions

In summary, ACC particles with diameter of about 300 nm are synthesized first. Then we have investigated the phase transition process from ACC to crystalline phase on chitin film by adding WSM or magnesium ion in aqueous solution. WSM may stabilize ACC, and the existence of WSM and chitin film leads to form the rod-like aragonite crystal aggregates. Comparatively, the collaborative effect of magnesium ion and chitin film not only induces to form the aragonite crystal aggregates, but also inhibits the transformation from ACC to Mg-calcite. A possible growth mechanism of the aragonite crystal aggregates with different morphologies is thereby proposed. This study may give some useful clues for understanding the biomineralization process of $CaCO_3$ in nature. Furthermore, the present work provides some new insights into preparation of $CaCO_3$ aggregates with complex shape and fine structure assembled from amorphous precursor.

Acknowledgements

The authors are grateful for the financial support from National Natural Science Foundation of China (51361130032, 51472139) and Doctor Subject Foundation of the Ministry of Education of China (20120002130002).

REFERENCES

1. F. C. Meldrum, H. Coelfen, *Chemical Reviews*, 2008, **108**, 4332-4432.
2. F. C. Meldrum, *International Materials Reviews*, 2003, **48**, 187-224.
3. J. Aizenberg, D. A. Muller, J. L. Grazul, D. R. Hamann, *Science*, 2003, **299**, 1205-1208.
4. S. Raz, P. C. Hamilton, F. H. Wilt, S. Weiner, L. Addadi, *Adv Funct Mater*, 2003, **13**, 480-486.
5. E. Beniash, J. Aizenberg, L. Addadi, S. Weiner, *P Roy Soc B-Biol Sci*, 1997, **264**, 461-465.
6. I. M. Weiss, N. Tuross, L. Addadi, S. Weiner, *J Exp Zool*, 2002, **293**, 478-491.
7. J. Aizenberg, G. Lambert, L. Addadi, S. Weiner, *Adv Mater*, 1996, **8**, 222-226.
8. L. Addadi, S. Raz, S. Weiner, *Adv Mater*, 2003, **15**, 959-970.

9. J. Aizenberg, S. Weiner, L. Addadi, *Connect Tissue Res*, 2003, **44**, 20-25.
10. Y. Politi, T. Arad, E. Klein, S. Weiner, L. Addadi, *Science*, 2004, **306**, 1161-1164.
11. Y. Politi, R. A. Metzler, M. Abrecht, B. Gilbert, F. H. Wilt, I. Sagi, L. Addadi, S. Weiner, P. U. P. A. Gilbert, *P Natl Acad Sci USA*, 2008, **105**, 20045-20045.
12. P. K. Ajikumar, L. G. Wong, G. Subramanyam, R. Lakshminarayanan, S. Valiyaveettil, *Cryst Growth Des*, 2005, **5**, 1129-1134.
13. J. Liu, S. Pancera, V. Boyko, J. Gummel, R. Nayuk, K. Huber, *Langmuir*, 2012, **28**, 3593-3605.
14. K. Sawada, *Pure Appl Chem*, 1997, **69**, 921-928.
15. N. Koga, Y. Z. Nakagoe, H. Tanaka, *Thermochim Acta*, 1998, **318**, 239-244.
16. R. S. K. Lam, J. M. Charnock, A. Lennie, F. C. Meldrum, *Crystengcomm*, 2007, **9**, 1226-1236.
17. S. F. Chen, J. H. Zhu, J. Jiang, G. B. Cai, S. H. Yu, *Adv Mater*, 2010, **22**, 540-545.
18. Y. Nishino, Y. Oaki, H. Imai, *Cryst Growth Des*, 2009, **9**, 223-226.
19. J. Jiang, M. R. Gao, Y. H. Qiu, S. H. Yu, *Nanoscale*, 2010, **2**, 2358-2361.
20. C. Gunther, A. Becker, G. Wolf, M. Epple, *Z Anorg Allg Chem*, 2005, **631**, 2830-2835.
21. T. Kato, *Adv Mater*, 2000, **12**, 1543-1546.
22. S. Raz, S. Weiner, L. Addadi, *Adv Mater*, 2000, **12**, 38-42.
23. N. A. J. M. Sommerdijk, E. N. M. van Leeuwen, M. R. J. Vos, J. A. Jansen, *Crystengcomm*, 2007, **9**, 1209-1214.
24. E. Loste, R. M. Wilson, R. Seshadri, F. C. Meldrum, *J Cryst Growth*, 2003, **254**, 206-218.
25. X. R. Xu, A. H. Cai, R. Liu, H. H. Pan, R. K. Tang, K. W. Cho, *J Cryst Growth*, 2008, **310**, 3779-3787.
26. L. Liu, B. Hu, S. F. Chen, S. J. Liu, J. Jiang, G. B. Cai, S. H. Yu, *Crystengcomm*, 2010, **12**, 3593-3598.
27. X. Geng, L. Liu, J. Jiang, S. H. Yu, *Cryst Growth Des*, 2010, **10**, 3448-3453.
28. Y. Y. Liu, J. Jiang, M. R. Gao, B. Yu, L. B. Mao, S. H. Yu, *Cryst Growth Des*, 2013, **13**, 59-65.
29. S. Albeck, S. Weiner, L. Addadi, *Chem-Eur J*, 1996, **2**, 278-284.
30. Y. Ma, S. R. Cohen, L. Addadi, S. Weiner, *Adv Mater*, 2008, **20**, 1555-1559.
31. Z. J. Ma, J. Huang, J. Sun, G. N. Wang, C. Z. Li, L. P. Xie, R. Q. Zhang, *J Biol Chem*, 2007, **282**, 23253-23263.
32. A. P. Wheeler, K. W. Rusenko, D. M. Swift, C. S. Sikes, *Mar Biol*, 1988, **98**, 71-80.
33. Y. Zhang, L. P. Xie, Q. X. Meng, T. M. Jiang, R. L. Pu, L. Chen, R. Q. Zhang, *Comp Biochem Phys B*, 2003, **135**, 565-573.
34. N. Nassif, N. Pinna, N. Gehrke, M. Antonietti, C. Jager, H. Colfen, *P Natl Acad Sci USA*, 2005, **102**, 12653-12655.
35. I. M. Weiss, V. Schonitzer, *J Struct Biol*, 2006, **153**, 264-277.
36. J. Aizenberg, G. Lambert, S. Weiner, L. Addadi, *J Am Chem Soc*, 2002, **124**, 32-39.
37. Y. F. Ma, L. Qiao, Q. L. Feng, *Mat Sci Eng C-Mater*, 2012, **32**, 1963-1970.
38. B. Borzecka-Prokop, A. Weselucha-Birczynska, E. Koszowska, *J Mol Struct*, 2007, **828**, 80-90.
39. D. Di Tommaso, N. H. de Leeuw, *Phys Chem Chem Phys*, 2010, **12**, 894-901.
40. Y. F. Ma, Y. H. Gao, Q. L. Feng, *Mat Sci Eng C-Mater*, 2011, **31**, 1338-1342.
41. G. Wolf, C. Gunther, *J Therm Anal Calorim*, 2001, **65**, 687-698.
42. N. V. Vagenas, C. G. Kontoyannis, *Vib Spectrosc*, 2003, **32**, 261-264.
43. G. Behrens, L. T. Kuhn, R. Ubic, A. H. Heuer, *Spectr. Lett.*, 1995, **28**, 983-995.
44. W. Z. Wang, G. H. Wang, Y. K. Liu, C. L. Zheng, Y. J. Zhan, *J Mater Chem*, 2001, **11**, 1752-1754.

45. A. Anderson, *Spectr. Lett.*, 1996, **29**, 819-825.
46. I.-Y. Kim, S.-J. Seo, H.-S. Moon, M.-K. Yoo, I.-Y. Park, B.-C. Kim, C.-S. Cho, *Biotechnology advances*, 2008, **26**, 1-21.
47. 刘旭杰，高永华，冯庆玲，*复合材料学报*, 2012, **29**, 21-27.
48. F. Nudelman, B. A. Gotliv, L. Addadi, S. Weiner, *J Struct Biol*, 2006, **153**, 176-187.
49. J. M. Alia, Y. D. de Mera, H. G. M. Edwards, P. G. Martin, S. L. Andres, *Spectrochim Acta A*, 1997, **53**, 2347-2362.
50. M. Faatz, F. Grohn, G. Wegner, *Adv Mater*, 2004, **16**, 996-1000.
51. A. Mucci, *Am J Sci*, 1983, **283**, 780-799.
52. D. Gebauer, A. Volkel, H. Colfen, *Science*, 2008, **322**, 1819-1822.
53. J. Mahamid, A. Sharir, L. Addadi, S. Weiner, *P Natl Acad Sci USA*, 2008, **105**, 12748-12753.
54. X. Long, Y. Ma, L. Qi, *Cryst Growth Des*, 2011, **11**, 2866-2873.
55. G. Falini, S. Fermani, M. Gazzano, A. Ripamonti, *J Mater Chem*, 1998, **8**, 1061-1065.
56. S. Weiner, L. Addadi, *J Mater Chem*, 1997, **7**, 689-702.
57. H. Tang, J. G. Yu, X. F. Zhao, *Mater Res Bull*, 2009, **44**, 831-835.
58. H. Nebel, M. Epple, *Z Anorg Allg Chem*, 2008, **634**, 1439-1443.
59. N. Xu, Y. Li, L. Zheng, Y. Gao, H. Yin, J. Zhao, Z. Chen, J. Chen, M. Chen, *Chemical Engineering Journal*, 2014, **251**, 102-110.
60. J. D. Rodriguez-Blanco, S. Shaw, P. Bots, T. Roncal-Herrero, L. G. Benning, *J Alloy Compd*, 2012, **536**, S477-S479.
61. M. Faatz, F. Grohn, G. Wegner, *Mat Sci Eng C-Bio S*, 2005, **25**, 153-159.
62. Y. Politi, D. R. Batchelor, P. Zaslansky, B. F. Chmelka, J. C. Weaver, I. Sagi, S. Weiner, L. Addadi, *Chem Mater*, 2010, **22**, 161-166.
63. S. H. Yu, H. Colfen, M. Antonietti, *J Phys Chem B*, 2003, **107**, 7396-7405.
64. X. H. Jiang, M. B. Zheng, H. Q. Chen, L. J. Pan, J. Tao, J. M. Cao, *J Inorg Mater*, 2008, **23**, 1283-1286.

Figure Captions

Figure 1. Characterization of the prepared amorphous calcium carbonate. (a) SEM image; (b) X-ray pattern; (c) FT-IR spectra; (d) TGA-MS curve.

Figure 2. Raman spectrograms of $CaCO_3$ crystals with the different morphologies transformed from ACC particles under the control of water soluble matrix or magnesium ion on silicon slice or chitin film in aqueous solution. (a) calcite; (b) Mg-calcite; (c) aragonite; (d) aragonite; (e) and (f) are the magnified peaks indicated by the black arrows in (c) and (d) respectively. The inset in each figure indicates the typical crystal morphology.

Figure 3. SEM images of $CaCO_3$ crystals transformed from ACC particles in aqueous solution with or without water soluble matrix at room temperature for 12 h. (a) crystal growth without WSM on silicon slice, calcite precipitated; (b) crystal growth without WSM on chitin film, calcite precipitated; (c) crystal growth with WSM on silicon slice, calcite and aragonite precipitated; (d) crystal growth with WSM on chitin film, aragonite precipitated. The scale bars in the whole micrographs are 3 μm.

Figure 4. SEM images of $CaCO_3$ crystals transformed from ACC particles under control of magnesium ion at room temperature for 12 h. (a) $[Mg^{2+}]$=10 mM, silicon slice; Mg-calcite and aragonite precipitated; (b) $[Mg^{2+}]$=10 mM, chitin film; aragonite precipitated; (c) $[Mg^{2+}]$=40 mM, silicon slice; Mg-calcite and aragonite precipitated; (d) $[Mg^{2+}]$=40 mM, chitin film; aragonite precipitated. The scale bars in the whole micrographs are 3 μm.

Figure 5. SEM images of ACC crystallization process occurring on chitin film under the control of water soluble matrix or magnesium ion. (a) the original ACC particles; crystallization process with WSM at (b) 6 h #ACC and aragonite# and (c) 12 h #aragonite#; crystallization process with magnesium ion at (d) 2 h #Mg-ACC#, (e) 6 h #aragonite#, (f) 12 h [mg^{2+} ion concentration: 10 mM] #aragonite# and (i) 12 h [mg^{2+} ion concentration: 40 mM] #aragonite#; (g) EDX result of the sample. The square area in (d) indicates the analysis location; (h) SAED pattern of the precipitate in (d). ## indicates the crystal polymorph of the precipitated $CaCO_3$.

Figure 6. Schematic illustration of ACC crystallization process occurring on chitin film under the control of (a) water soluble matrix or (b) magnesium ion.

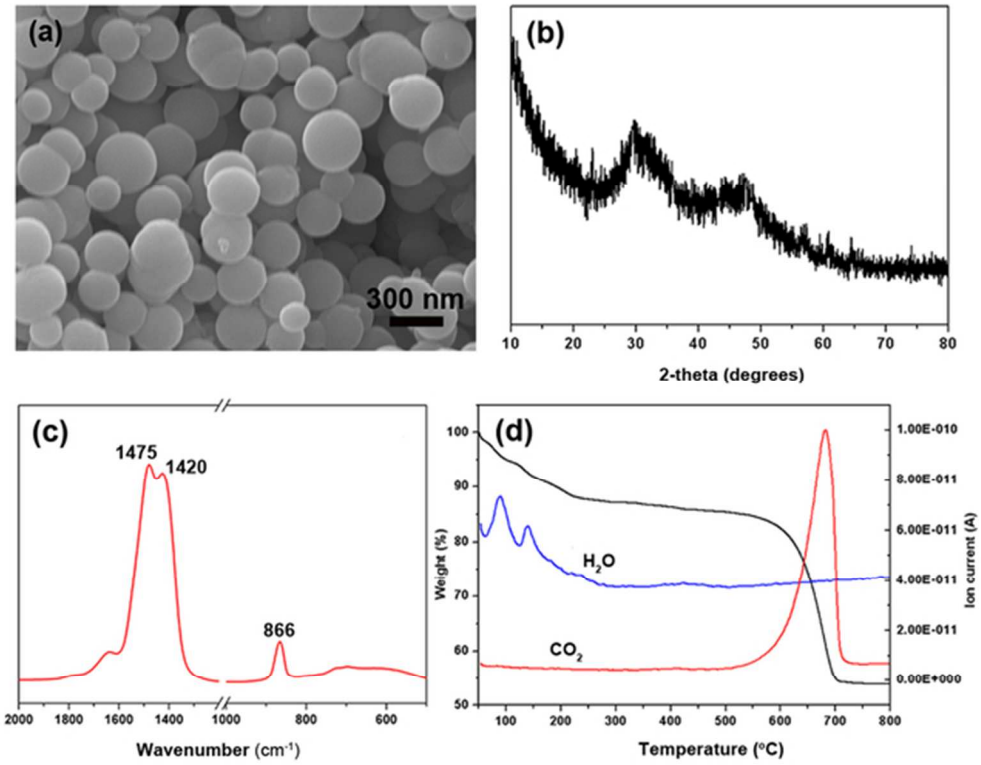

Figure 1. Characterization of the prepared amorphous calcium carbonate. (a) SEM image; (b) X-ray pattern; (c) FT-IR spectra; (d) TGA-MS curve.
54x43mm (300 x 300 DPI)

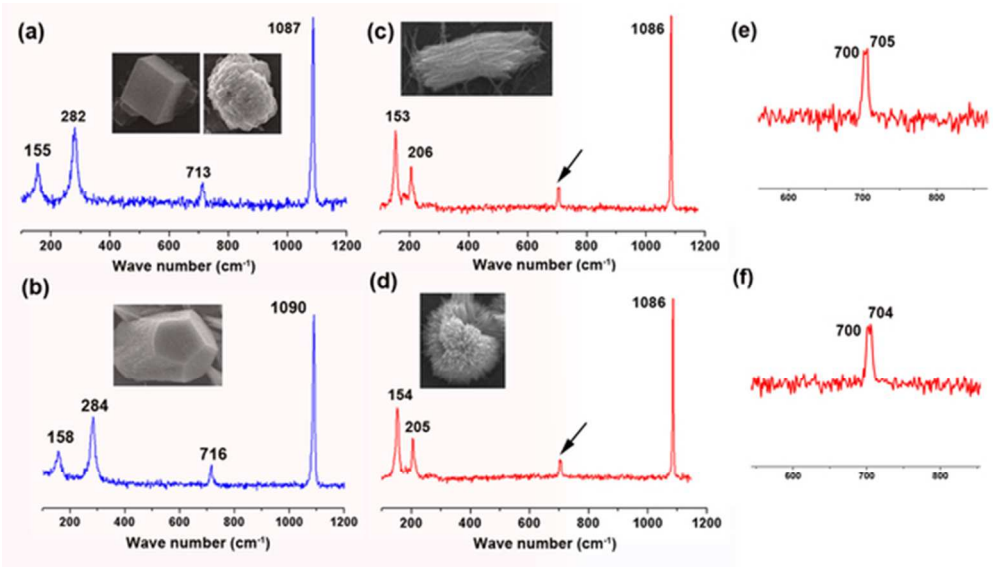

Figure 2. Raman spectrograms of CaCO3 crystals with the different morphologies transformed from ACC particles under the control of water soluble matrix or magnesium ion on silicon slice or chitin film in aqueous solution. (a) calcite; (b) Mg-calcite; (c) aragonite; (d) aragonite; (e) and (f) are the magnified peaks indicated by the black arrows in (c) and (d) respectively. The inset in each figure indicates the typical crystal morphology.
53x30mm (300 x 300 DPI)

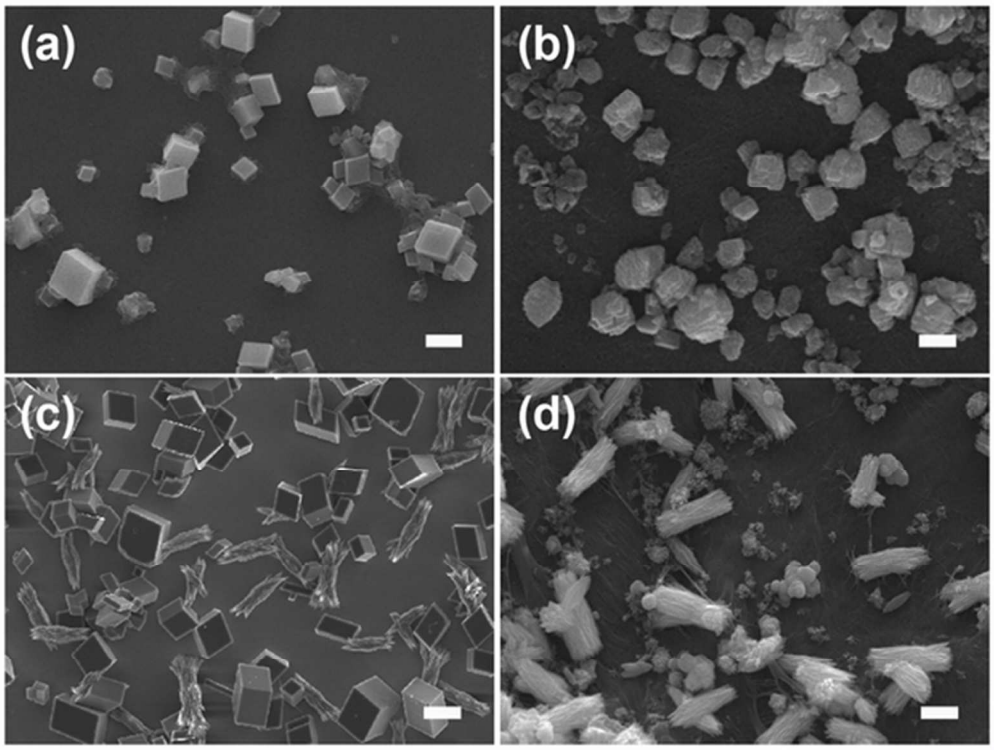

Figure 3. SEM images of CaCO3 crystals transformed from ACC particles in aqueous solution with or without water soluble matrix at room temperature for 12 h. (a) crystal growth without WSM on silicon slice, calcite precipitated; (b) crystal growth without WSM on chitin film, calcite precipitated; (c) crystal growth with WSM on silicon slice, calcite and aragonite precipitated; (d) crystal growth with WSM on chitin film, aragonite precipitated. The scale bars in the whole micrographs are 3 μm.
52x39mm (300 x 300 DPI)

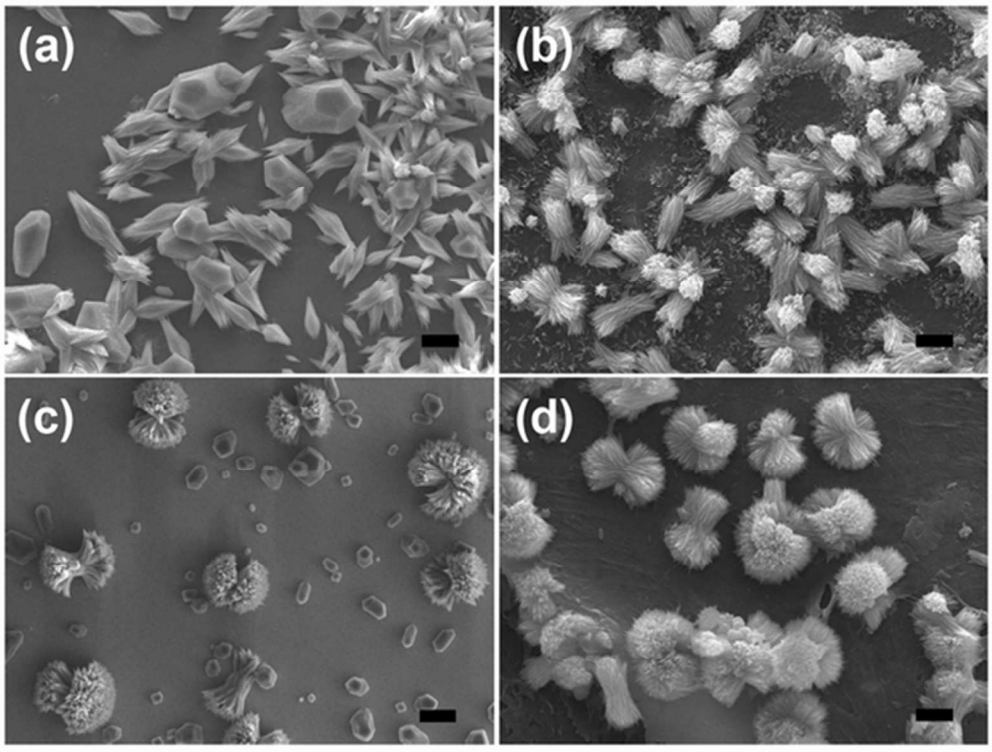

Figure 4. SEM images of CaCO3 crystals transformed from ACC particles under control of magnesium ion at room temperature for 12 h. (a) [Mg2+]=10 mM, silicon slice; Mg-calcite and aragonite precipitated; (b) [Mg2+]=10 mM, chitin film; aragonite precipitated; (c) [Mg2+]=40 mM, silicon slice; Mg-calcite and aragonite precipitated; (d) [Mg2+]=40 mM, chitin film; aragonite precipitated. The scale bars in the whole micrographs are 3 μm.
52x39mm (300 x 300 DPI)

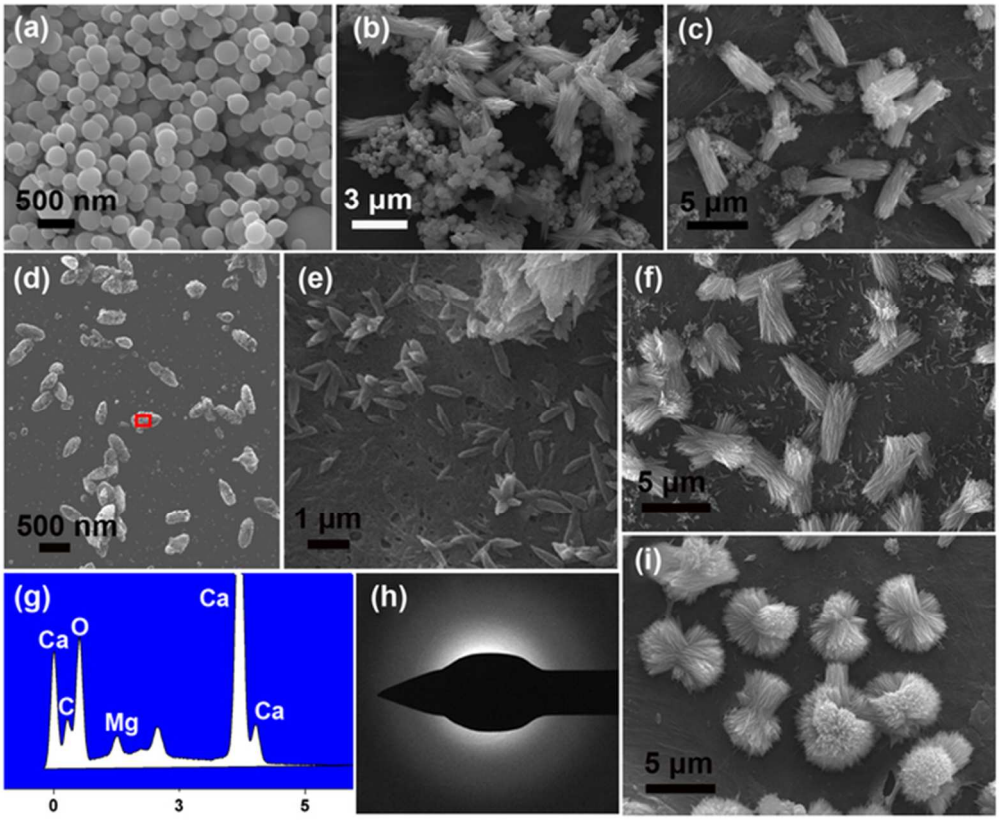

Figure 5. SEM images of ACC crystallization process occurring on chitin film under the control of water soluble matrix or magnesium ion. (a) the original ACC particles; crystallization process with WSM at (b) 6 h #ACC and aragonite# and (c) 12 h #aragonite#; crystallization process with magnesium ion at (d) 2 h #Mg-ACC#, (e) 6 h #aragonite#, (f) 12 h [mg2+ ion concentration: 10 mM] #aragonite# and (i) 12 h [mg2+ ion concentration: 40 mM] #aragonite#; (g) EDX result of the sample. The square area in (d) indicates the analysis location; (h) SAED pattern of the precipitate in (d). ## indicates the crystal polymorph of the precipitated CaCO3.
57x47mm (300 x 300 DPI)

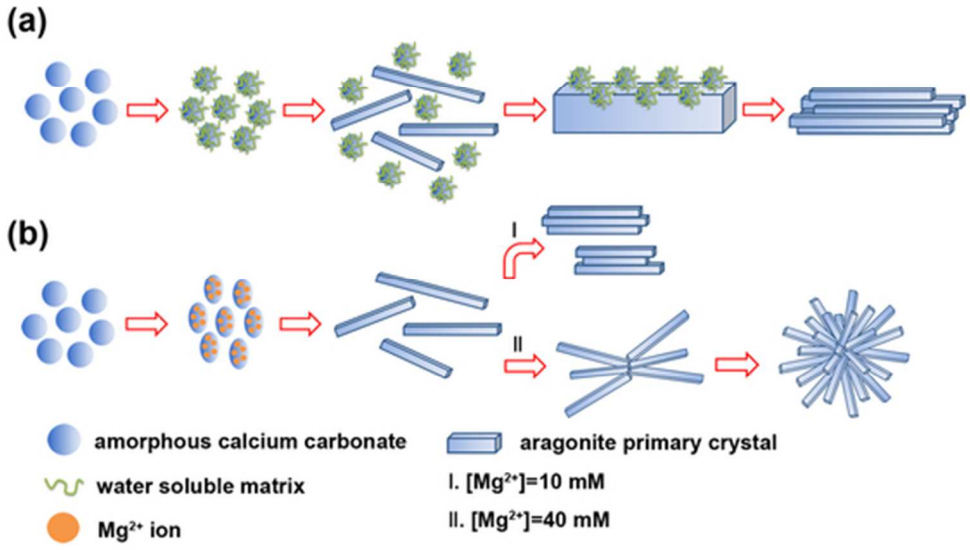

Figure 6. Schematic illustration of ACC crystallization process occurring on chitin film under the control of (a) water soluble matrix or (b) magnesium ion.
49x28mm (300 x 300 DPI)